A IJRDO Journal of Applied Science
ISSN:2455-6653
Review Article

SYNTHESIS, CHARACTERIZATION AND THERMAL ANALYSIS OF EUROPIUM AND TERBIUM DOPED LANTHANUM BASED COMPOUNDS

[1]Harshad Trivedi, [2*]Vimal Joshi, [3]Kevil Shah, [4]B S Chakrabarty, [5]Ronak Patel, [6]S H Chaki, [7]M P Deshpande

[1]Department of Physics, Shri R. K. Parikh Arts & Science College, Petlad, Gujarat.
[2]*Department of Physics, Shri R. K. Parikh Arts & Science College, Petlad, Gujarat.Email id: tharshad98@gmail.com
[3,4]Department of Applied Physics, Maharaja Sayaji Rao University, Vadodara.
[5]Department of Chemistry, Sardar Patel University, Anand.
[6,7]Department of Physics, Sardar Patel University, Anand.

Abstract
Three host matrices namely of Lanthanum namely Lanthanum Oxide (La2O3), Lanthanum Oxysulphide (La2O2S) and Lanthanum Phosphate (LaPO4) were taken for this study. Each of these host matrices were activated by Europium (Eu) and Terbium (Tb) in different concentrations, thus generating six set of samples. The samples were characterized by X ray diffraction. The d values were found to be matching with the respective JCPDS values. Doping being in minuscule proportions did not alter the peak positions. Thermal analyses confirm the high thermal stability of all doped compounds. The observed weight gain at higher temperatures is credibly attributed to the incorporation of nitrogen species into lattice voids during high-temperature exposure in the inert environment, which is likely to enhance the thermal robustness and structural integrity of the materials.

Key Words: Lanthanum Phosphate, Terbium, Thermal analyses, minuscule, incorporation

DOI: https://doi.org/10.69980/as.v12i2.6698
Received 28 February 2026 | Accepted 25 May 2026 | Published 6 June 2026

INTRODUCTION

Lanthanum based compounds, particularly Oxides, Sulphides and phosphates are a versatile class of materials.[1] In their pristine form, they are primarily used for their high-temperature stability, basicity, and dielectric properties. The high stability makes them suitable for use in high-temperature environments. Their physical, thermal, and chemical stability, make them suitable for structural and high-temperature uses, making them superior to many other host materials.[2]

They are used extensively in their pure state for a host of applications like inert carrier for catalysts in chemical reactions due to their stability and high surface area, proton conductor in intermediate-temperature fuel cells for their high thermal stability and low toxicity, oxidative coupling of methane to produce ethylene, due to their basicity and thermal stability, thin-film transistors and capacitors as a high k- dielectric layer to replace SiO2, ferroelectric materials as an additive to improve capacitance, glass manufacturing to improve the refractive index and lower the dispersion of optical lenses in camera lenses and night-vision devices, X-ray imaging and CRT lighting as a host matrix for rare-earth ions to create light emitting materials, create infrared-transmitting optical ceramics with a high cut-off wavelength and IR-to-Visible conversion and UV detection, among others.[3]

The doped versions of these compounds have specific properties, which can be further modified by the extent of doping. Doping can create oxygen vacancies and improve surface reactivity. Doping introduces defect sites and improves conductivity, enabling specialized applications.[4] Doping with trivalent rare-earth ions (Ln3+) activates inner 4f shell transitions, making them exceptionally efficient for optical applications. Lanthanum-doped materials, including modifications of phosphate, are highly effective as adsorbents for removing phosphate from wastewater.[5]

Experimental

The $La_2O_3:Eu^{3+}$/Tb3+ phosphor samples were synthesized using the conventional Solid-state (Ceramic) method. Lanthanum Nitrate Hexahydrate [$La(NO_3)_3 \cdot 6H_2O$] was taken for the host matrix. Europium Nitrate Hexahydrate [$Eu(NO_3)_3 \cdot 6H_2O$] or Terbium Nitrate Hexahydrate [Tb $(NO_3)_3 \cdot 6H_2O$] was taken as dopants for activation of the phosphor samples. All these precursors were in powder form. Stoichiometric amounts of these nitrates were taken based on the required doping concentration (e.g., 1 mole %), by accurately weighing them on the analytical balance. The precursor powders were put in an agate mortar and pestle to grind them uniformly. Ethanol in appropriate quantity was used to turn it into a homogenous mixture paste. This process involved around an hour of grinding and mixing, as homogeneity aids in improved reactivity of the precursors.

In order to remove the ethanol, moisture and other residual solvents, the mixture paste was dried in a hot air oven at 150 °C for 4 hours. Small chunks were formed on drying. They were crushed and grinded again. The resulting powders for samples with different dopant concentrations were put in alumina crucibles for heating at high temperature to enable the solid-state reaction. These crucibles were transferred in a programmable muffle furnace for them to be

heated at 1100 °C for 4 hours. It took several hours for the furnace to reach 1100 °C, after which it was held for 4 hours. The high temperature heating also enables the decomposition of nitrate precursors and the release of gaseous byproducts, which are primarily the oxides of Nitrogen (NO_x). Subsequently, the heating facilitates the initiation of solid-state reaction and leading to crystallization of the required products i.e. La_2O_3\:Eu^{3+} and $La_2O_3:Tb^{3+}$. After holding at 1100 °C, the furnace was allowed to cool naturally for 48 hours, for it to reach room temperature. The resulting product was a hard chunk inside the crucibles. These chunks were carefully taken out from the crucibles into an agate mortar and pastel to be ground again to obtain a fine, uniform

powder. These powders were kept in airtight desiccators for characterization and analysis.

2La (NO3)3·6H2O+Eu (NO3)3·6H2O La2O3:Eu3++6NO2+3/2O2+18H2O

2La (NO3)3·6H2O+Tb (NO3)3·6H2O La2O3:Tb3++6NO2+3/2O2+18H2O

The La_2O2S: Eu^{3+}/Tb3+ phosphor samples were synthesized using the same Solid-state (Ceramic) method, with an additional precursor. Lanthanum Nitrate Hexahydrate [$La(NO_3)_3 \cdot 6H_2O$] was taken for the host matrix. Europium Nitrate Hexahydrate [Eu $(NO_3)_3 \cdot 6H_2O$] or Terbium Nitrate Hexahydrate [Tb $(NO_3)_3 \cdot 6H_2O$] was taken as dopants for activation of the phosphor samples. In addition, Thaiourea [CH_4N_2S] was taken as the source of Sulphur. It also acts as a fuel to aid the attainment of high temperature. The synthesis of Oxysulphides generally involves heating under a mildly reducing atmosphere, which can be done either by flowing a reducing gas mixture e.g. N_2/H_2 or by using the decomposition gases of Thaiourea itself. The sulfur released from Thaiourea facilitates the formation of the Oxysulfide.

The high temperature heating enables the decomposition of nitrate precursors and the release of gaseous byproducts, which are primarily the oxides of Nitrogen (NO_x) and Sulphur (SO_x). Subsequently, the heating facilitates the initiation of solid-state reaction and leading to crystallization of the required products i.e. La_2O2S :Eu^{3+} and La_2O2S:Tb^{3+}.

2La(NO3)3·6H2O+Eu(NO3)3·6H2O+6CH4N2S
La2O2S:Eu3++9N2+6CO2+6SO2
+36H2O

2La(NO3)3·6H2O+ Tb (NO3)3·6H2O+6CH4N2S La2O2S:
Tb3++9N2+6CO2+6SO2
+36H2O

For the synthesis of LaPO4:Eu^{3+}/Tb3+ phosphor samples, Lanthanum Nitrate Hexahydrate [$La(NO_3)_3 \cdot 6H_2O$] was taken for the host matrix. Europium Nitrate Hexahydrate [$Eu(NO_3)_3 \cdot 6H_2O$] or Terbium Nitrate Hexahydrate [Tb $(NO_3)_3 \cdot 6H_2O$] was taken as dopants for activation of the phosphor samples. Diammonium hydrogen phosphate [$(NH_4)_2HPO_4$] was added to incorporate the phosphate content needed for $LaPO_4$ formation.

La(NO3)3·6H2O+ Eu(NO3)3·6H2O+2(NH4)2HPO4
  LaPO4:Eu3++6NO2+2P2
O5+8NH3+18H2O

La(NO3)3·6H2O+ Tb (NO3)3·6H2O+2(NH4)2HPO4
  LaPO4:Tb3++6NO2+2P2O5
+8NH3+18H2O

The characterization of the synthesized material was done using the technique of X-ray Diffraction, which is an elementary technique for characterization of solid samples. It reveals the nature of the material including its crystal structure, type and other characteristics.

The phosphor samples synthesized for these studies were subjected to the same technique to get their X-ray powder diffractograms on a Rigaku, Japan make Miniflex model X-ray diffractometer. All diffraction patterns were obtained using Cu Kα radiation (λ = 1.54051 A°), at 30 kV and 15 mA. Measurements were taken in the pertinent 2θ ranges varying between 10° and 70° with steps of 0.02°.

The three host matrices namely of Lanthanum namely Lanthanum Oxide (La2O3), Lanthanum Oxysulphide (La2O2S) and Lanthanum Phosphate (LaPO4) were taken for this study, as the presence of dopant/activator in such minuscule quantities is not expected to result into any significant deviation in the XRD pattern. The results have been found to be on the expected lines. 'd' values of the peaks were calculated using the Bragg's equation. These values were considered for matching with the JCPDS/ICDD files and other references in literature to ascertain the h, k, l values and other parameters.

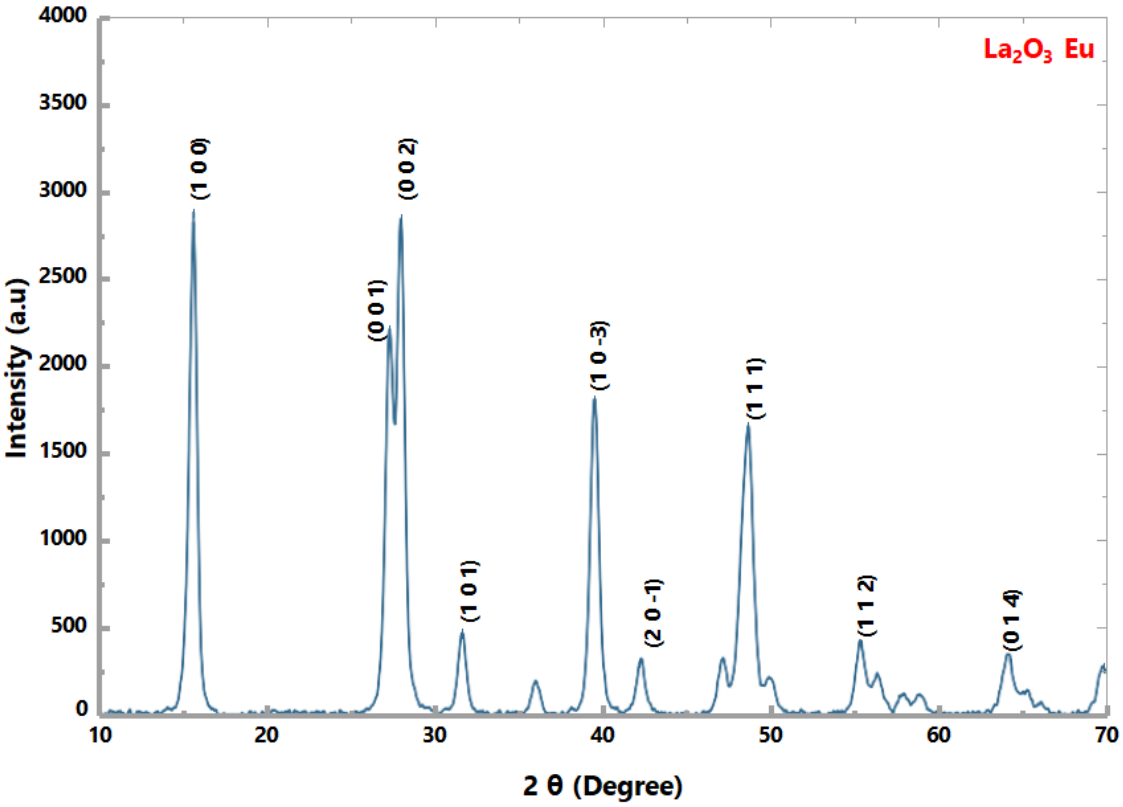

Fig 1: XRD pattern of La2O3

The XRD pattern of La2O3 exhibits sharp peaks showing a high degree of crystallinity. The peaks were found to be in closely matching with JCPDS cards 83-1345 and 40-1279 as well as other publications.[6] La2O3 is found in hexagonal as well as cubic phases, with the former being the prominent phase.

The hexagonal phase represents the A-type $M2O3$ with space group $P\bar{6}2m$, corresponding to JCPDS 40-1279 and is the most commonly observed low-temperature and stable phase.

The cubic phase represents the C-type $M2O3$ with space group la-3 also exists and is referenced by other file numbers, such as JCPDS 04-0856 or 83-1344. This phase of La2O3 is obtained by only specific synthesis methods or by temperature treatment of samples.

The highest intensity is at the 2Θ values of 15.6º and 27.96º corresponding to the (001) and (100) orientations respectively, which are the dominating peaks. The samples are polycrystalline. Other peaks also have relatively high intensity. The specific lattice parameters i.e. a and c values, which range around $a \approx 3.93$ Å and $c \approx 6.13$ Å vary with synthesis methods and conditions. The peaks in can be indexed to the hexagonal phase of La2O3. The lattice constants were found to be a = 4.03 Å, b = 4.03 Å and c = 6.403 Å, with the cell volume being 103.99 Å^3.

The XRD pattern of La2O2S also exhibits sharp peaks showing a high degree of

crystallinity. The peaks were found to be closely matching with JCPDS cards 75-1954 and 27-0263 as well as literature.[7] La2O2S exists in hexagonal phase with the space group $P\bar{3}m1$.

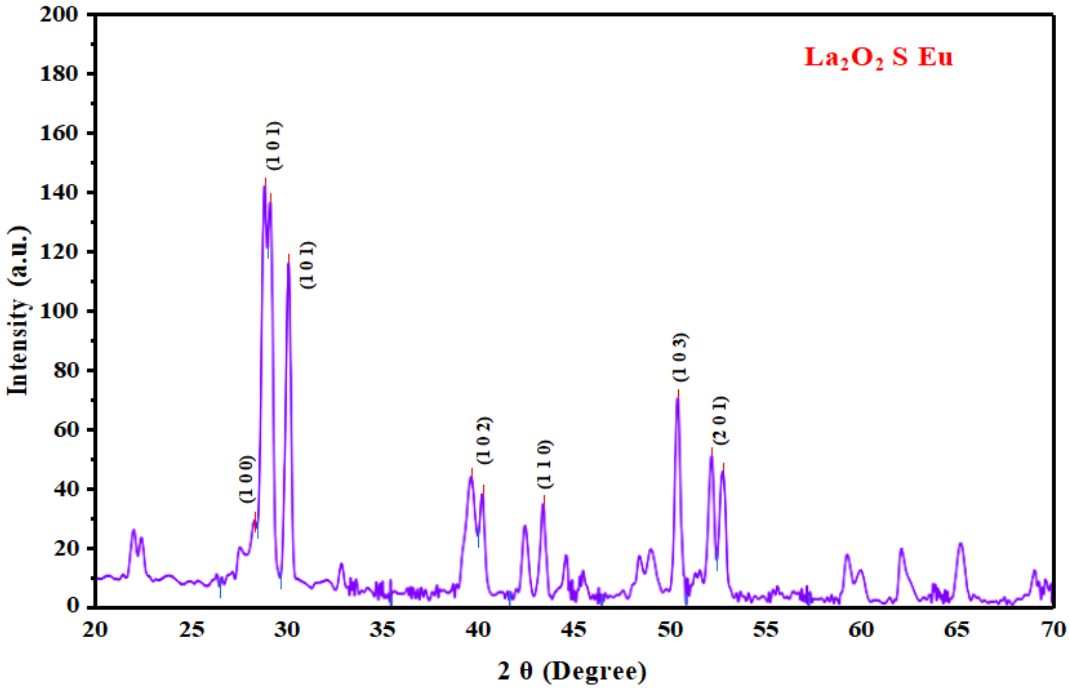

Fig 2: XRD pattern of La2O2S

The highest intensities are at the 2Θ values of 28.84º and 30.1º corresponding to the (100) and (101) orientations respectively. They are the dominating peaks. Other peaks have relatively low intensities. The samples are polycrystalline. The values of lattice parameters were found to be a = b = 3.73 A° & c = 7.40 A° with a cell volume 102.95 Å^3

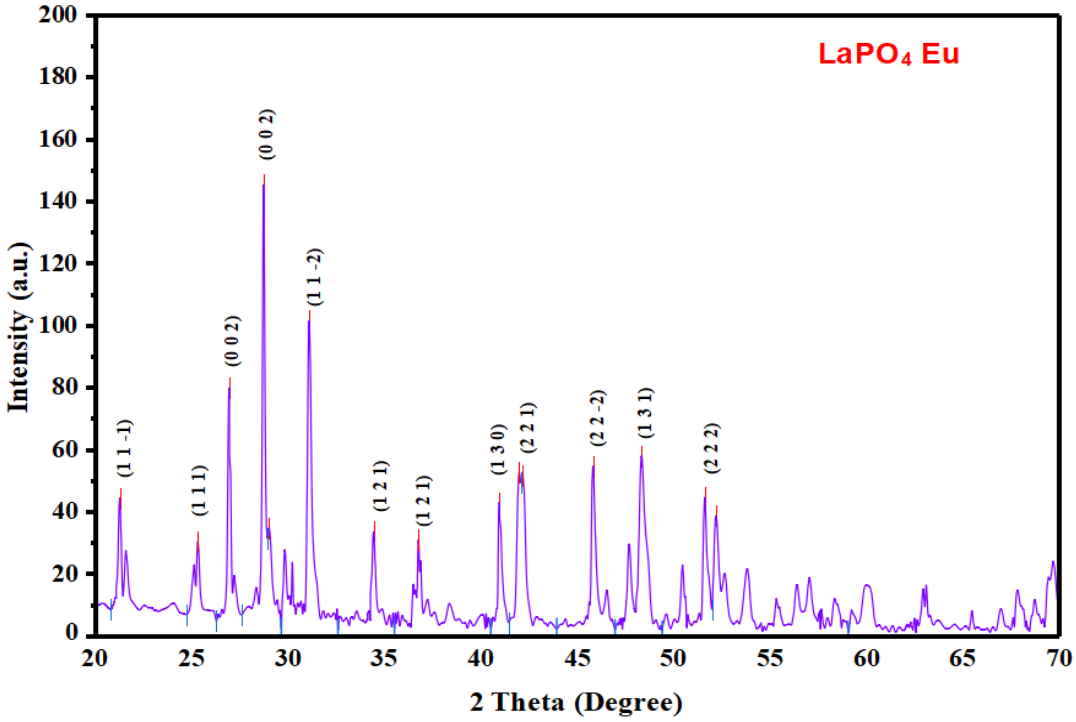

Fig 3: XRD pattern of LaPO4

The XRD pattern of LaPO4 exhibit sharp peaks showing a high degree of crystallinity. The peaks were found to be closely matching with JCPDS cards 46-1439 as well as other references.[8] It corresponds to hexagonal lanthanum phosphate hydrate (LaPO4·0.5H2O), which has a rhabdophane structure with the space Group *P*6222.

The highest peaks are at 2θ value of around 28.8° corresponding to the hkl plane (2 0 0) for both the samples. The values of lattice parameters calculated from the peaks, were found to be a = b = 3.73 A°& c = 7.40 A°.

This hexagonal phase is metastable and typically transforms into the monoclinic monazite phase upon heating above 600--800ºC. The standard values of this phase are given by the JCPDS file 32-0493 or 35-0731.
The synthesized samples, after being characterized by X ray diffraction, need to be checked for their thermal stability. This is done by using thermal analysis techniques, which refer to a variety of techniques in which a property of the sample is continuously measured by subjecting the sample through a predetermined temperature profile. Although there are a handful of such techniques, one of the most common includes Thermal Gravimetric Analysis (TA). In TA the mass loss versus increasing temperature of the sample is recorded. The basic instrumental requirements are simple: a precision balance, a programmable furnace, and a recorder. Modern instruments, however, tend to be automated and include software for data reduction. In addition, provisions are made for surrounding the sample with an air, nitrogen, or an oxygen atmosphere. It is widely used as a quality control technique for industrial, pharmaceutical, electronic and other applications.[9]
The thermal stability and decomposition behavior of all synthesized samples doped with Europium and Terbium were studied using Thermo Gravimetric Analysis (TGA), Differential Thermal Gravimetry (DTG and Differential Thermal Analysis (DTA). The data were acquired using a Seiko SII-EXSTAR TG/DTA-7200 thermal analyzer under an inert nitrogen (N_2) atmosphere at a constant flow rate of 100 mL/min. The heating rate was maintained at 10 K/min, and the temperature range extended from room temperature to 1270 K. All thermal profiles were recorded simultaneously for comparative assessment. The TG, DTG and DTA curves offer detailed insight into some of the thermal characteristics of the synthesized Eu- and Tb-doped rare-earth compounds.

The samples were evaluated to determine their thermal stability. Each sample was heated from room temperature to 1273 K at a constant rate of 10 K/min under a nitrogen flow rate of 100 mL/min.

Eu-doped La2O3

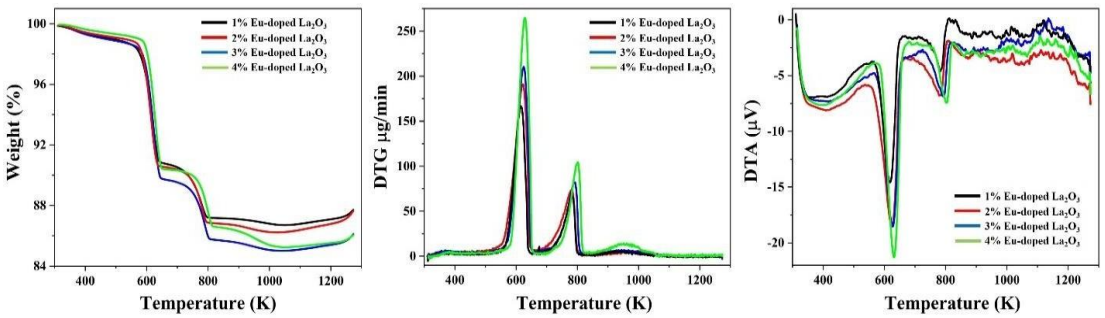

Figure 4 (a) TG curve (b) DTG curve and (c) DTA curve for Eu-doped La2O3 samples

The TG curves shown in Figure 4(a) exhibit a four-step weight loss profile, indicating the presence of different thermally removable species and intermediate phases during the decomposition process.

In the low-temperature region (300–570 K), all samples show a minor weight loss which can be attributed to the removal of physically adsorbed moisture and weakly bound surface hydroxyl groups [10]. The small magnitude of weight loss and the nearly overlapping TG curves suggest that this stage is largely independent of Eu concentration.

In the second stage (571–640 K) significant weight loss is observed for all compositions. This stage is associated with the decomposition of lanthanum hydroxide species and the removal of chemically bound hydroxyl groups [11,12]. Moderate Eu incorporation enhances the extent of hydroxide formation or its subsequent decomposition, while at higher doping, partial stabilization of the structure may slightly reduce this contribution.

The third stage from 641–800 K, is associated with the conversion of intermediate oxy-carbonate species ($La_2O_2CO_3$) into the stable oxide phase. Eu incorporation influences the formation and stability of carbonate intermediates [10].

In the high-temperature region from 801–1273 K, no major decomposition is expected. The minor variations can be attributed to subtle structural rearrangements, densification, or instrumental effects such as buoyancy corrections at high temperatures. The absence of significant mass loss in this region indicates that the decomposition process is largely completed below 800 K [10].

The differential thermogravimetric (DTG) profiles exhibit two primary decomposition peaks along with a minor high-temperature features.

The low-temperature region (~300–550 K) is largely independent of Eu concentration. The DTG peak around ~600–620 K is attributed to the rapid decomposition of lanthanum hydroxide species and the removal of chemically bound hydroxyl groups. Increased doping of Eu accelerates the kinetics of decomposition. This is attributed to the higher density of surface defects and lattice strain introduced by Eu^{3+} ions, which act as active sites to facilitate the rapid release of hydroxyl groups. The primary reason for the increased defect density is that the substitution of the larger La^{3+} (0.116 nm) with the smaller Eu^{3+} (0.106 nm) creates a size mismatch that induces local lattice contraction and structural distortion [13]. Eu doping influences both the kinetics (rate) and extent (amount) of decomposition differently. A broader peak in the ~750–800 K region is associated with the decomposition of intermediate carbonate species such as lanthanum oxycarbonate. At higher temperatures (above ~800 K) also, an extended decomposition of deep-seated residues is indicated.

Overall, the DTG analysis reveals the dual role of Eu in modifying both the rate and pathway of thermal decomposition.

The differential thermal analysis (DTA) curves of Eu-doped La_2O_3 samples exhibit distinct endothermic features that correspond closely with the multi-step decomposition behavior observed in the TG and DTG analysis.

A weak and broad endothermic feature in the low-temperature region (300–550 K), is attributed to the desorption of physically adsorbed moisture and loosely bound surface hydroxyl groups.

A prominent endothermic peak in the ~580–640 K range corresponds to the decomposition of lanthanum hydroxide species and the removal of chemically bound hydroxyl groups. Eu incorporation enhances the rate of heat absorption and decomposition kinetics.

In the intermediate temperature region (~650–800 K), a second endothermic peak is attributed to the decomposition of intermediate carbonate species such as lanthanum oxycarbonate. At higher temperatures (above ~800 K), the DTA curves gradually approach a baseline. The DTA behavior highlights a clear distinction between the decomposition kinetics (rate) and the extent of decomposition (mass loss).

As shown in Figure 5(a) thermogravimetric (TG) curves of all Tb-doped La2O3 samples exhibit the same four-step decomposition trend. The similar behavior of the TG profiles in the low-temperature region suggests that Tb incorporation does not significantly alter the surface adsorption characteristics.

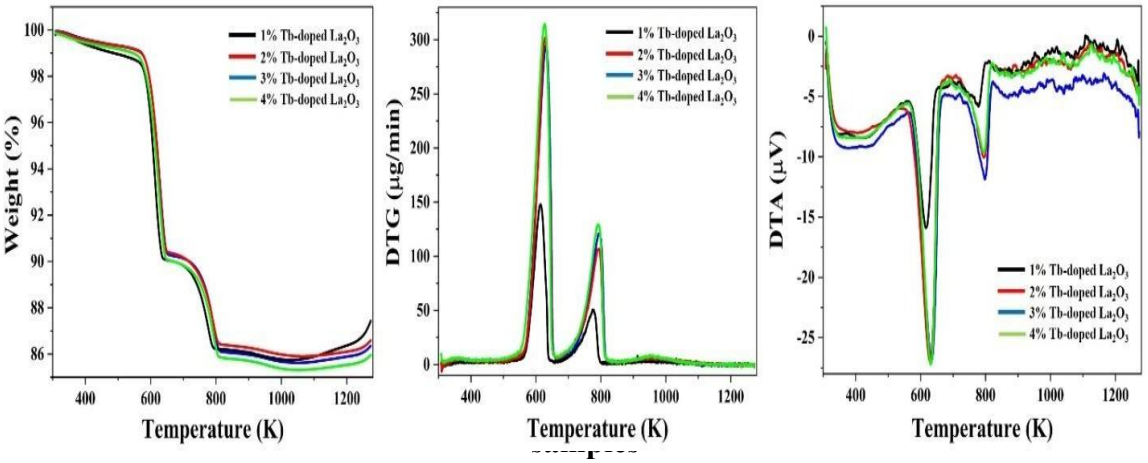

The initial mass reduction from 300 to 560 K is attributed to the removal of physically adsorbed moisture and weakly bound surface hydroxyl groups.

A sharp and dominant weight loss occurs in the step 2 from 561 to 640 K range, is associated with the decomposition of lanthanum hydroxide species (La(OH)3 → LaOOH → La2O3) and the removal of chemically bound hydroxyl groups [12]. The sharp nature of the weight loss indicates a rapid and energetically significant transformation.

In temperature region from 641–800 K, a moderate weight loss is observed for all the samples. This region is associated with the decomposition of intermediate lanthanum oxy-carbonate species (La2O2CO3) into the stable oxide phase [10]. This region shows a clear increasing trend of weight loss with Tb concentration (4% >3% >2% >1%), indicating that higher Tb incorporation promotes the formation or stabilization of carbonate-like intermediates.

In the high-temperature region (801–1273 K), a unique compositional dependence is observed. At low doping level, the La2O3 lattice maintains a higher degree of long-range order but likely retains a small fraction of residual intermediate species (such as oxy-carbonates) that exhibit slower decomposition kinetics [14]. As the temperature exceeds 1000 K, these species undergo a final, rapid structural reorganization and densification. The behavior indicates that increasing Tb concentration facilitates more complete and kinetically favorable decomposition, while lower doping levels retain intermediate phases that contribute to anomalous mass response at elevated temperatures.

The differential thermogravimetric (DTG) curves of all four Tb-doped La2O3 samples provide detailed insight into the rate of mass loss and clearly show the multi-step decomposition behavior observed in the TG analysis. The DTG analysis confirms that the decomposition kinetics of Tb-doped La2O3 is strongly dependent on composition, with non-uniform behavior across different stages. The DTG profiles are characterized by two prominent peaks corresponding to the major decomposition stages, along with minor features at higher temperatures.

The differential thermal analysis (DTA) curves of Tb-doped La2O3 samples correlate well with the multi-step decomposition behavior observed in the TG and DTG profiles.

In the low-temperature region (~300–550 K), a weak endothermic feature is observed for all compositions, corresponding to the initial weight loss in the TG curves. A prominent endothermic peak in the ~580–640 K range is observed for all samples, which is associated with the decomposition of lanthanum hydroxide species and the removal of chemically bound hydroxyl groups.

In the intermediate temperature region (~650–800 K), a second endothermic feature is observed, is attributed to the decomposition of residual carbonate species. At higher temperatures (~800–1273 K), the DTA curves tend toward a near-baseline behavior, indicating the absence of major decomposition events.

Overall, the DTA analysis confirms that the thermal decomposition of Tb-doped La2O3 is predominantly endothermic in nature, governed by the removal of hydroxide and carbonate species. The compositional dependence observed across different temperature regions further supports the conclusion that Tb incorporation influences the decomposition pathway in a stage-dependent manner, with lower doping favoring hydroxide retention and higher doping promoting more complete and kinetically favorable transformation.

The thermogravimetric (TG) behavior of Eu-doped La2O2S along with the DTG and DTA curves are shown in Figure 6.

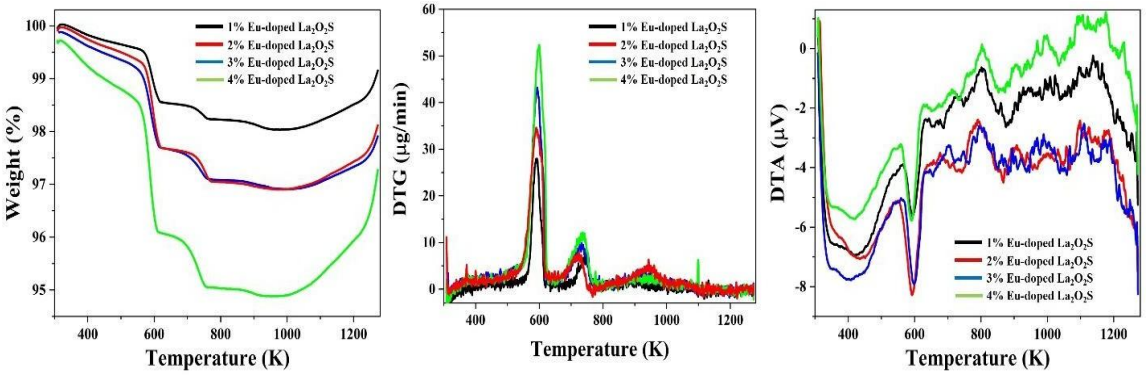

Figure 6 (a) TG curve (b) DTG curve and (c) DTA curve for Eu-doped La2O2S samples

In step 1 from 300K to 550K, all samples exhibit minor weight loss due to the removal of physically adsorbed moisture and weakly bound surface molecules. The step 2, from 551 K to 610 K correspond to the primary decomposition step involving residual precursor species and sulfur-related volatile components [17]. The 4% Eu-doped sample shows comparatively higher weight loss than the other compositions, suggesting that higher dopant concentration introduces greater lattice distortion and defect sites, which accommodate a larger amount of thermally unstable species. Step 3, from 610 K to 750 K, associated with the continued removal of residual species and the onset of structural relaxation indicates that decomposition is more extended and occurs over a wider temperature range. In the final stage, from 751 K to 1273 K, no major phase transformation has been observed. This region is primarily associated with lattice stabilization, defect annihilation, and possible densification processes.

DTG profiles indicate the temperatures at which the rate of decomposition is maximum. In the lower temperature region (~300–500 K), the DTG signal is broad and of very low intensity, indicating a slow and continuous mass loss associated with desorption of surface-bound species. The peak intensity in the region ~580–610 K follows the order: 4% > 3% > 2% > 1%. It also suggests that decomposition occurs at high rate in this composition. The rate of decomposition in the region ~700–750 K is comparatively low. No major decomposition process occurs at higher temperatures (>800 K) due to slow structural rearrangement.

In the low-temperature region (~300–500 K), a broad endothermic behavior is observed for all the samples. This behavior is attributed to the removal of physically adsorbed moisture and weakly bound surface species.

A sharp endothermic peak is observed in the temperature range of ~550–610 K, corresponding to the primary decomposition process. This thermal event represents the

main decomposition stage involving the removal of residual precursor species and sulfur-related volatile components. The increase in DTG peak intensity with dopant concentration of Eu (4% > 3% > 2%
> 1%) indicates that the rate of mass loss increases with Eu incorporation. This behavior suggests that, despite higher mass loss and decomposition rate, the energy required for decomposition is reduced at higher dopant concentrations due to increased lattice disorder and weak bonding due to ionic radius mismatched between La3+ and Eu3+ [13].
Overall, the DTA results, in correlation with TG and DTG analyses, demonstrate that the thermal behavior of Eu-doped La2O2S is governed by the combined effects of endothermic decomposition and exothermic structural relaxation. Also, it can be said that as the Eu concentration increases, both the amount and rate of mass loss increase, while the energy required for decomposition decreases and exothermic processes due to defects become more significant at higher temperatures.
Tb-doped La2O2S

The thermogravimetric (TG) behavior of Tb-doped La2O2S along with the DTG and DTA curves are shown in Figure 7.

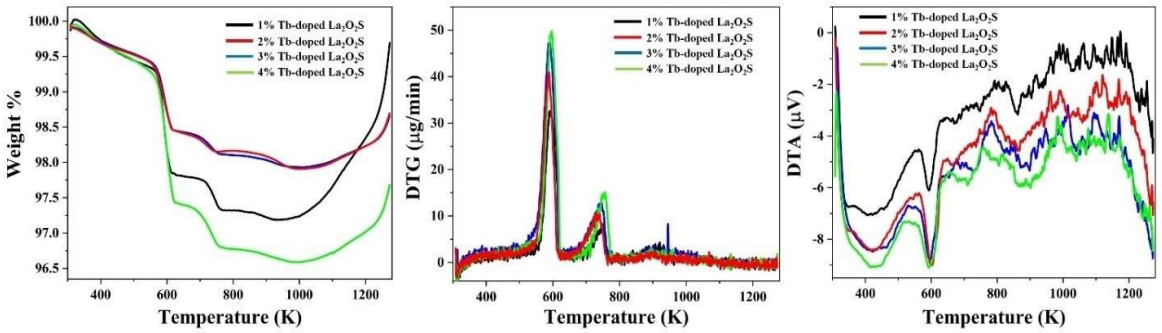

Figure 7 (a) TG curve (b) DTG curve and (c) DTA curve for Tb-doped La2O2S samples

In initial temperature range from 300–560 K, all samples showed a minor and gradual weight loss. This initial mass reduction is attributed to the removal of physically adsorbed moisture and surface-bound gaseous species. The nearly overlapping nature of the TG curves in this region suggests that Tb incorporation has minimal influence on the surface adsorption characteristics of the material.
Step-2 from 550–610 K, corresponds to the primary decomposition of residual precursor species and unreacted sulfur-related volatile components trapped within the lattice during the synthesis process [17]. The increased weight loss in the 1%-doped sample relative to the 2%- and 3%-doped compositions can be attributed to a critical dopant threshold or "dilute limit" effect [15,16]. At very low concentrations (1%), the Tb ions may initially act as nucleating centers that facilitate a higher entrapment of volatile species during crystal growth compared to the intermediate 2% and 3% concentrations. As the concentration increases to 2% and 3%, a temporary stabilization or "lattice contraction" effect may occur, slightly improving the purity or density of the host matrix. However, once the concentration reaches 4% doping, the increased lattice distortion and surface defect density become the dominant factors again, leading to the highest observed weight loss. The subsequent steps display a continued but comparatively moderate to low weight loss, indicating the completion of major decomposition processes and the onset of structural stabilization, where the lattice undergoes rearrangement toward a more thermodynamically stable configuration.
The DTG curves for all samples provide further insight into the rate of decomposition. Unlike the TG curves, the DTG profiles do not distinctly separate all four stages but instead show dominant peaks corresponding to the primary decomposition events. The DTG analysis confirms that increasing Tb concentration increases the rate of

decomposition, particularly in the primary degradation region.
The DTA curves of Tb-doped La2O2S also support the thermal events observed in the TG and DTG analyses by providing information on the energetic nature of the thermal processes.

The initial low-temperature region (300–560 K) shows endothermic behavior for all samples. A sharp and well-defined endothermic peak is observed in the temperature region of 560-610K, where thermal energy is used to break the chemical bonds of residual precursors and volatile sulfur compounds.
Interestingly, while the 4% Tb-doped sample shows the highest mass loss, its DTA peak is relatively broader and less intense than those of the lower-doped samples. Higher Tb incorporation introduces significant lattice distortion and strain. This pre-existing structural disorder weakens the overall bonding environment of the host matrix, effectively lowering the localized energy barriers required for decomposition. Consequently, the decomposition occurs more "easily" (over a wider range) rather than in one synchronized energy burst.
At higher temperatures, the DTA curves show a continued but less intense exothermic trend.
The thermogravimetric behavior of Eu and Tb doped LaPO4 are given below in Figure 8(a).

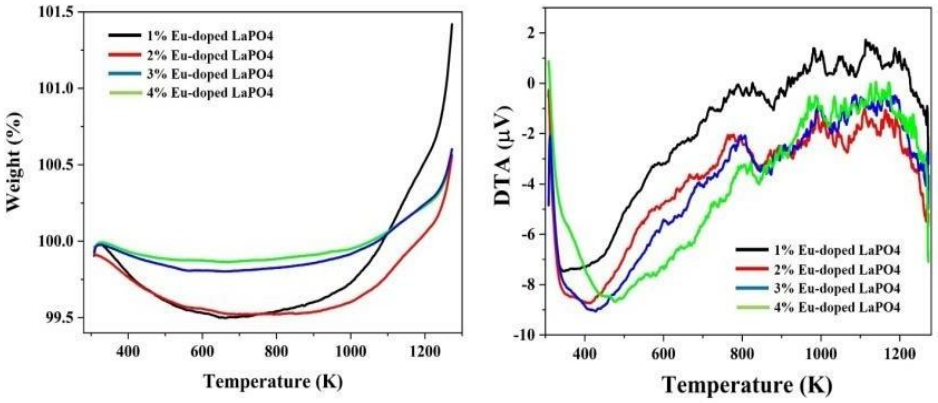

Figure 8 (a) TG curve and (b) DTA curve for Eu-doped LaPO4 samples.

In the initial temperature region from ~300–700 K, all samples show a minor weight loss, which can be due to the evaporation of physically adsorbed moisture and surface-bound hydroxyl groups [18].
The middle temperature ranges from 700 to 900 K display a plateau-like behavior, showing the absence of major decomposition processes and confirming the intrinsic thermal stability of the LaPO4 host lattice.
At higher temperature range >900 K, a gradual increase in the recorded weight is observed for all samples. The weight gains observed in this temperature range can be due to N2 entrapment within the generated voids of samples [19].
Eu incorporation significantly influences the thermal stability of LaPO4, with optimal stability observed in the 3–4% doping range. Also, the absence of significant decomposition confirms the excellent thermal robustness of Eu-doped LaPO4 for high-temperature applications.
The DTA behavior exhibits initial endothermic behavior followed by multiple broad exothermic dips without any sharp phase transition peaks, confirming the thermal stability of the LaPO4 host lattice in the investigated temperature range.

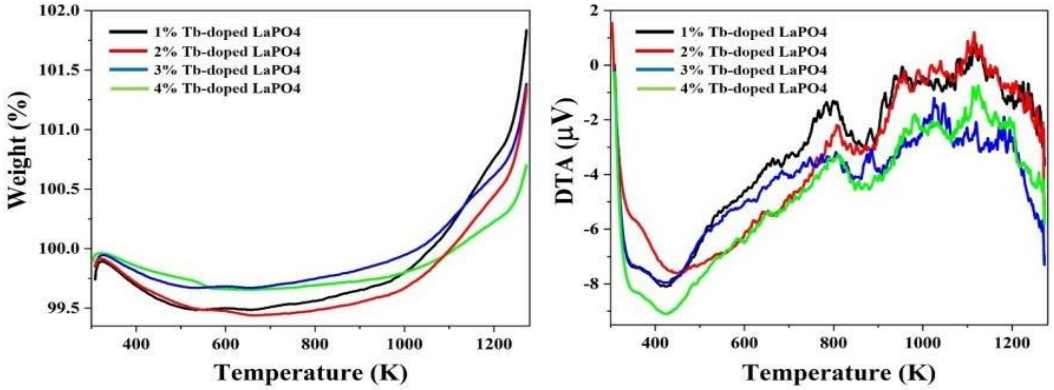

Figure 9 (a) TG curve and (b) DTA curve for Tb-doped LaPO4 samples.

All four compositions displayed a nearly identical weight-loss profile regardless of the dopant concentration.
In the initial temperature region from ~300–600 K, all samples show a minor weight loss of ~0.5%. This corresponds to the evaporation of surface-adsorbed moisture and the removal of residual hydroxyl groups or organic solvents used during the synthesis process.
The intermediate temperature ranges from ~600K-950K, exhibit a plateau region, indicating that the thermal stability of material.

Above 950K, a notable weight gain is observed for all four samples. The weight gains observed in this temperature range can be due to N2 entrapment within the generated voids of samples [19].
The DTA curves of all compositions shows broad features without any sharp, high-intensity peaks associated with first-order phase transitions, confirming the high thermal stability of the LaPO4 host lattice within the investigated temperature range.
The above results underscore the exceptional thermal robustness of the Tb-doped LaPO4 material, making it suitable for applications involving high thermal loads.
The DTG results exhibit noisy behavior. Hence they have been treated separately.
The curves show the DTG curves for Eu-doped and Tb-doped samples.

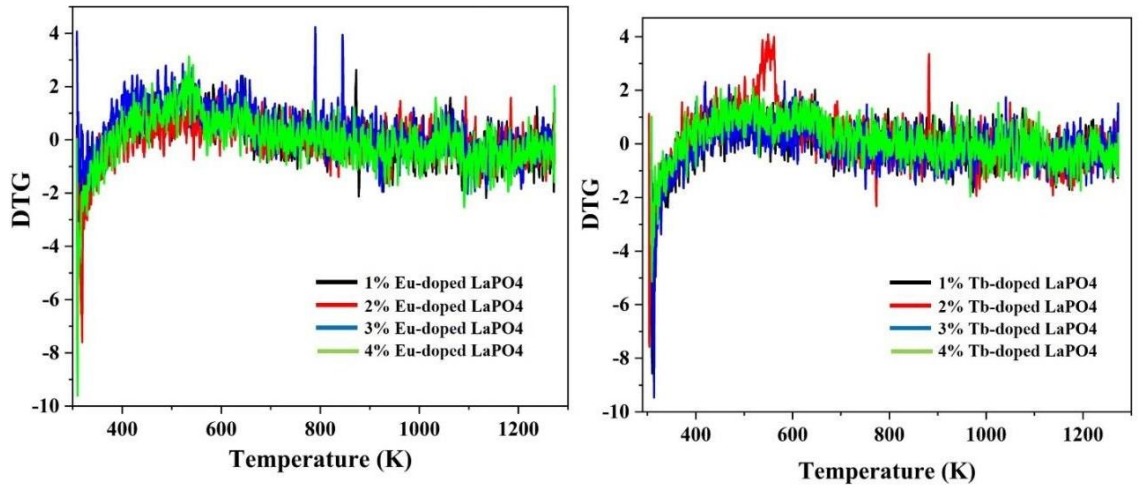

Figure 10 (a) DTG curve for Eu-doped LaPO4 and (b) DTG curve for Tb-doped LaPO4.

The DTG curves for both Eu-doped and Tb-doped LaPO4 samples provide a more localized view of the rate of mass change during heating.
The high-frequency fluctuations (spikes) observed in this region does not correspond to any physical decomposition or phase changes. Instead, they are attributed to the limits of

instrumental sensitivity when measuring nearly negligible mass changes. Given that the total weight loss is extremely low, the signal-to-noise ratio in the derivative curve becomes more prominent. The absence of any significant, broad negative peaks after 500K confirms that the material does not undergo any secondary decomposition or oxygen loss, further reinforcing the high thermal stability discussed in the TG section.

CONCLUSION

The characterization of the samples using XRD establishes that they are polycrystalline compounds with high crystallinity and the peak values match with the respective references of JCPDS files as well as other relevant publications. The thermal analyses confirm the high thermal stability of all doped compounds. The consistent and complementary nature of the TG/DTG/DTA profiles across all samples validates the reliability of the results. The observed minor weight gain at higher temperatures is credibly attributed to the incorporation of nitrogen species into lattice voids during high-temperature exposure in the inert environment, which may enhance the thermal robustness and structural integrity of the materials.

REFERENCES:

1. Rani, S., Nair, M. T. S., & Nair, P. R. (2015). Lanthanum-based oxides: Synthesis, properties and applications—A review. Journal of Alloys and Compounds, 633, 154–172. https://doi.org/10.1016/j.jallcom.2015.02.114
2. Ghosh, S., & Patra, A. (2018). Lanthanum sulfides: Synthesis, properties and applications. Materials Today Chemistry, 9, 56–74. https://doi.org/10.1016/j.mtchem.2018.01.005
3. Peng, B., Li, Y., Huo, L., et al. (2017). Lanthanum phosphates: Structure, luminescence and applications in solid-state lighting and bioimaging. Chemical Society Reviews, 46(13), 3887–3936. https://doi.org/10.1039/C6CS00936J
4. Tong, H., Ouyang, S., Bi, Y., et al. (2020). Recent advances in lanthanum-based compounds (oxides, sulfides, phosphates): Synthesis, properties and photocatalytic applications. Coordination Chemistry Reviews, 405, 213139.
5. https://doi.org/10.1016/j.ccr.2019.213139
6. Zhang, H., Gong, M., & Liu, X. (2021). Lanthanum-based materials: From oxides and sulfides to phosphates—A review of structures, properties and emerging applications. Journal of Materials Chemistry A, 9(26), 14806–14839. https://doi.org/10.1039/D1TA01978A
7. Yu, L., Han, Y., Lin, R., Ge, K., Zhang, C., Zhang, J., & Jia, G. (2021). Controllable synthesis and luminescence properties of one-dimensional La2O3 and La2O3:Ln3+ (Ln = Er, Eu, Tb) nanorods with different aspect ratios. Journal of Luminescence, 229, 117663. https://doi.org/10.1016/j.jlumin.2020.117663
8. Shah, Kevil & Ćirić, Aleksandar & Murthy, K.V.R. & Chakrabarty, B.S.. (2020). Investigation of a new way of synthesis for Nano crystallites of La2O2S & 1%Ln3+ (Ln = Pr, Eu, Tb, Dy, Er) doped La2O2S and study their structural and optical properties. Journal of Alloys and Compounds. 851. 156725. 10.1016/j.jallcom.2020.156725.
9. Li, J., Dong, H., Yang, F., Sun, L., Zhao, Z., Bai, R., & Zhang, H. (2019). Simple Preparation of LaPO4:Ce, Tb Phosphors by an Ionic-Liquid-Driven Supported Liquid Membrane System. International Journal of Molecular Sciences, 20(14), 3424. https://doi.org/10.3390/ijms20143424
10. Skoog, D. A., West, D. M., Holler, F. J., & Crouch, S. R. (2014). Fundamentals of analytical chemistry (9th ed.). Brooks/Cole.
11. Khalaf, W. M., & Al-Mashhadani, M. H. (2022). Synthesis and characterization of lanthanum oxide la2o3 net-like nanoparticles by new combustion method. Biointerface Research in Applied Chemistry, 12(3), 3066–3075.

https://doi.org/10.33263/BRIAC123.30663075
12. Méndez, M., Carvajal, J. J., Marsal, L. F., Salagre, P., Aguiló, M., Díaz, F., Formentín, P., Pallarès, J., & Cesteros, Y. (2013). Effect of the La(OH)3 preparation method on the surface and rehydroxylation properties of resulting La2O3 nanoparticles. Journal of Nanoparticle Research, 15(3). https://doi.org/10.1007/s11051-013-1479-7
13. Kang, J. G., Kim, Y. Il, Won Cho, D., & Sohn, Y. (2015). Synthesis and physicochemical properties of La(OH)3 and La2O3 nanostructures. Materials Science in Semiconductor Processing, 40, 737–743. https://doi.org/10.1016/j.mssp.2015.07.050
14. Vinothkumar, G., Rengaraj, S., Arunkumar, P., Cha, S. W., & Suresh Babu, K. (2019). Ionic Radii and Concentration Dependency of RE3+ (Eu3+, Nd3+, Pr3+, and La3+)-Doped Cerium Oxide Nanoparticles for Enhanced Multienzyme-Mimetic and Hydroxyl Radical Scavenging Activity. Journal of Physical Chemistry C, 123(1), 541–553. https://doi.org/10.1021/acs.jpcc.8b10108
15. Thesis Author, D. (n.d.). ETH Library In-situ High-Resolution X-ray Spectroscopy of Light Rare-Earth Compounds. https://doi.org/10.3929/ethz-b-000000059
16. Fengt, X.-Q., Tang$ T Shanghai, T. B., Lkpaament, W., Kong, H., Couege, B. K., & Tong, K. (1993). Mg-doping threshold effect and H-containing defects in LiNbO3 Shanghai uwx)sO. People's Republic of china (Vol. 5).
17. Ogale, S. B. (2010). Dilute doping, defects, and ferromagnetism in metal oxide systems. In Advanced Materials (Vol. 22, Number 29, pp. 3125–3155). https://doi.org/10.1002/adma.200903891
18. Tan, S., & Li, D. (2018). Enhancing Oxygen Storage Capability and Catalytic Activity of Lanthanum Oxysulfide (La2O2S) Nanocatalysts by Sodium and Iron/Sodium Doping. ChemCatChem, 10(3), 550–558. https://doi.org/10.1002/cctc.201701117
19. Gallini, S., Jurado, J. R., & Colomer, M. T. (2005). Combustion synthesis of nanometric powders of LaPO4 and Sr-substituted LaPO4. Chemistry of Materials, 17(16), 4154–4161. https://doi.org/10.1021/cm047945q
20. Patel, S., Chaki, S. H., & Vinodkumar, P. C. (2020). Thermal analysis of direct vapour transport technique grown tin selenide single crystals. Thermochimica Acta, 689. https://doi.org/10.1016/j.tca.2020.178614